Thermochimica Acta 511 (2010) 129–139

Contents lists available at ScienceDirect

Thermochimica Acta

journal homepage: www.elsevier.com/locate/tca

PLA nanocomposites: Effect of filler type on non-isothermal crystallization

G.Z. Papageorgiou [a], D.S. Achilias [a], S. Nanaki [a], T. Beslikas [b], D. Bikiaris [a,*]

[a] Laboratory of Polymer Chemistry and Technology, Department of Chemistry, Aristotle University of Thessaloniki, GR-541 24 Thessaloniki, Macedonia, Greece
[b] 2nd Orthopedic Department, Aristotle University of Thessaloniki, Greece

ARTICLE INFO

Article history:
Received 9 June 2010
Received in revised form 28 July 2010
Accepted 3 August 2010
Available online 11 August 2010

Keywords:
Poly(lactic acid)
Reinforcement ligaments
Silica nanoparticles
Montmorillonite
Multi-walled carbon nanotubes
Thermal characterization

ABSTRACT

Nanocomposites of poly(L-lactic acid) (PLA) with fumed silica nanoparticles (SiO_2), montmorillonite (MMT) and oxidized multi-walled carbon nanotubes (o-MWCNTs), containing 2.5 wt% nanoparticles were prepared, by solved evaporation method. SEM micrographs evidenced fine dispersion of the nanoparticles into PLA matrix. This has as result to act as efficient reinforcing agents increasing the storage modulus, as was verified from DMA analysis. The nanoparticles were found to be effective nucleaging agents in cases of silica nanoparticles and MWCNT. On cooling from the melt crystallization was accelerated by the presence of nanoparticles and the effective activation energy calculated using the isoconversional method of Friedmann decreased. The nucleation activity was calculated. Cold-crystallization was also affected by the presence of nanoparticles. However, it seems that the phenomenon begins at lower temperatures and this results in formation of imperfect crystalline structure which reduce macromolecular chain mobility of the remaining amorphous polymer, finally limiting the ultimate crystallinity.

1. Introduction

Biodegradable polyesters are materials that are hydrolysable at temperatures up to 50 °C (e.g., in composting) over a period of several months to one year [1,2]. Poly(lactic acid), (PLA), has proven to be the most attractive and useful biodegradable polymer among the numerous polyesters studied so far [3]. PLA is a biodegradable, biocompatible and compostable polyester derived from renewable resources such as corn, potato, cane molasses and beet sugar. It is a most promising environmentally friendly thermoplastic [4].

Commercially available high molecular weight PLA resins are produced via the lactide ring-opening polymerization route [5,6]. PLA has promising applications in packaging, consumer goods, fibers and in biomedicine because of its excellent mechanical properties, transparency, compostability and bio-safety [7–10].

The mechanical properties of high molecular weight PLA are comparable to other commodity thermoplastics like polystyrene and PET, and therefore it might replace these polymers for numerous applications [11,12]. But its high cost has limited its uses till recently. However, now latest technological advances have given rise to PLA resins that are commercially viable and can compete with petrochemical plastics [12–16].

Organic/inorganic nanocomposites are generally organic polymer composites with inorganic nanoparticles. The formation of hybrid organic/inorganic nanocomposite materials results in a synergetic effect of the two respective components in the nanometer scale leading to considerable improvements of various characteristics of the pristine organic material such as mechanical, thermal, and gas-barrier properties [17,18]. The small size of the fillers leads to a dramatic increase in interfacial area and this creates a significant volume fraction of interfacial polymer with properties different from the bulk polymer even at low loadings [19–22]. Typical filler amounts of less than 5 wt% result in effective enhancement of the nanocomposite [23]. There is a large variety of inorganic filler nanoparticles including nanotubes, layered silicates (e.g., montmorillonite, saponite), nanoparticles of metals (e.g., Au, Ag), metal oxides (e.g., TiO_2, Al_2O_3), semiconductors (e.g., PbS, CdS), and so forth [24].

In this work a series of PLA nanocomposites containing different types of inorganic filler nanoparticles were prepared, with constant filler content 2.5 wt% in every case, as in most cases a filler content of 2–3% leads to optimum properties [19–23]. Fillers include multi-walled carbon nanotubes, fumed silica and montmorillonite nanoparticles. The non-isothermal crystallization is studied in order to evaluate the effect of the type of filler. The study includes crystallization from the melt and from the glass (cold-crystallization). Various models are used to evaluate the nucleation efficiency of the fillers, the parameters of crystallization kinetics and the activation energy of the process.

2. Experimental

2.1. Materials

Commercially PLA reinforcement ligament for orthopedics applications under the trade name Resorbaid® was supplied from

* Corresponding author. Tel.: +30 2310 997812; fax: +30 2310 997769.
E-mail address: dbic@chem.auth.gr (D. Bikiaris).

0040-6031/$ – see front matter © 2010 Elsevier B.V. All rights reserved.
doi:10.1016/j.tca.2010.08.004

Cousin Biotech (France). Fumed silica (SiO_2) nanoparticles were supplied by Degussa AG (Hanau, Germany) under the trade name AEROSIL® 200, having a specific surface area of 200 m^2/g SiO_2 content >99.8% and average primary particle size 12 nm. Montmorillonite under the trade name Cloisite® 20A (org-MMT), which is modified with a dimethyl, dihydrogenated tallow quaternary ammonium chloride salt, was supplied from Southern Clay Products Inc. (Golzales, TX, USA). The particle sizes ranged between 2 and 13 nm and have modulus of elasticity 4.657 GPa, tensile strength 101 MPa and moisture content <2%. Multi-walled carbon nanotubes (MWCNTs) used in this work were synthesized by the chemical vapor deposition (CVD) process and were supplied by Nanothinx (Patras, Greece). Their diameter was between 9 and 20 nm, their length > 5 μm and were used in oxidized form (MWCNTs-COOH). For this reason, 1 g of the nanotubes were suspended in 40 ml of a mixture of concentrated nitric acid and sulfuric acid (1:3 in volume ratio) and refluxed for 15 min. After washing with deionized water until the supernatant had attained a pH around 7, the samples were dried under vacuum at 100 °C [25]. Dichloromethane anhydrous (≥99.8%) and tetrahydrofuran anhydrous (≥99.8%) were obtained from Aldrich Chemical Co.

2.2. Preparation of PLA nanocomposites

PLA ligament for orthopedic surgery applications was dissolved in a mixture of dichloromethane/tetrahydrofuran 50/50 (w/w) at room temperature while at the same mixture were dispersed different nanoparticles (SiO_2, montmorillonite or oxidized MWCNTs) under sonication for 1 h. The PLA solution and nanoparticles dispersion were mixed under stirring for 1 h and sonicated for additional 1 h. The mixture was cast on a Petri dish at room temperature. The solvent was allowed to evaporate in air for 3 days and then at 50 °C for 1 day in vacuum. Thus, after complete solvent removal thin films of the nanocomposites were obtained. The prepared films were placed in a desiccator to prevent any moisture absorption. Nanocomposites containing 2.5 wt% SiO_2, 2.5 wt% montmorillonite and 2.5 wt% oxidized MWCNTs were prepared with code names PLA/SiO_2, PLA/MMT and PLA/MWCNT.

2.3. Morphological examination

Electron diffraction (ED) and transmission electron microscopy (TEM) observations were made on ultra thin film samples of the various nanocomposites prepared by an ultramicrotome. These thin films were deposited on copper grids. ED patterns and TEM micrographs were obtained using a JEOL 120 CX microscope operating at 120 kV.

2.4. Dynamic mechanical analysis (DMA)

For dynamic thermomechanical analysis Rheometric Scientific analyzer (model Mk III) was used. The bending method was used at a frequency of 1 Hz, a strain level of 0.04% in the temperature range of 0–60 °C. The heating rate was 3 °C/min. Testing was performed using rectangular bars with dimensions, approximately, 30 mm × 10 mm × 3 mm.

2.5. Wide-angle X-ray diffraction (WAXD) study

X-ray diffraction measurements of the blends were performed by an automated Philipps PW1050 powder diffractometer, using nickel filtered Cu Ka radiation, at an angle of 2θ range 5–60°, with 0.028 step and 5 s data collection time.

2.6. Differential scanning calorimetry (DSC)

A PerkinElmer Pyris Diamond DSC differential scanning calorimeter, equipped with a PerkinElmer Intracooler II and calibrated with high purity indium and zinc standards was used for DSC measurements.

For non-isothermal crystallizations from the melt, low mass samples (about 5 mg) were first melted at 220 °C for 1 min and then cooled to 25 °C at various cooling rates, namely 2.5, 5, 7.5, 10, 15 and 20 °C/min. For non-isothermal crystallizations from the glass to record cold-crystallization, the samples were first melted at 220 °C for 1 min and then cooled to 25 °C at a rate 200 °C/min. Subsequently, heating scans at rates 2.5, 5, 7.5, 10, 15 and 20 °C/min were performed in the temperature range from 25 to 220 °C.

2.7. Polarizing light microscopy (PLM)

A polarizing light microscope (Nikon, Optiphot-2) equipped with a Linkam THMS 600 heating stage, a Linkam TP 91 control unit and a Jenoptic ProgRes C10Plus camera was used for PLM observations.

3. Results and discussion

3.1. Nanocomposites preparation and characterization

For nanoparticles surface-to-volume ratio plays a crucial role. While large surface-to-volume ratio makes nanoparticles superior reinforcements of polymer matrices over conventional fillers, it also brings difficulties in dispersing them due to the strong interactions among themselves. Due to these nanoparticle interactions, it is extremely difficult to disperse nanoparticles uniformly, specially at higher particle loadings. In a previous study, in order to enhance the compatibility between PLA and SiO_2 and to achieve a fine dispersion of SiO_2 into PLA matrix, L-lactic acid oligomers reacted onto the surface of silica nanoparticles before melt blending with PLA [26] The loading of SiO_2 nanoparticles in poly(L-lactide) (PLLA) matrix greatly improves the toughness and tensile strength of this material. Wu and Liao followed a different procedure according to which SiO_2 nanoparticles were well dispersed into PLA by using acrylic acid grafted polylactide (PLA-g-AA) as compatibilizer [27]. In the present study for the uniform dispersion of nanoparticles into PLA matrix the mixture of dichloromethane/tetrahydrofuran 50/50 (w/w) was chosen since from preliminary experiments it was found that nanoparticles are well dispersed avoiding precipitation.

As can be seen from Fig. 1a the SiO_2 nanoparticles were homogeneously dispersed into PLA. Taking into account that the average diameter of the used nanoparticles is 12 nm some aggregates were also observed with sizes less than 100 nm. In the case of montmorillonite (Fig. 1b) such aggregates were not observed, as well as in PLA/MWCNTs nanocomposite. From Fig. 1c it can be seen that MWCNTs are dispersed as individual nanotubes. This fine dispersion should be attributed to the interactions between the carboxyl groups of oxidized MWCNTs with hydroxyl end groups of PLA. Furthermore, as can be seen the MMT is dispersed in intercalated form into PLA matrix.

WAXD measurements of the as prepared films showed that they were essentially amorphous, since only the amorphous halo of PLA could be seen in the respective patterns.

Dynamic mechanical analysis is a useful and very sensitive technique for the investigation of microstructure of the macromolecular chain conformations and movements during the exposure of polymers to a variety of temperatures. In Fig. 2a are presented the storage modulus of neat PLA and its nanocomposites containing 2.5 wt% of different nanoparticles, as a function of temperature.

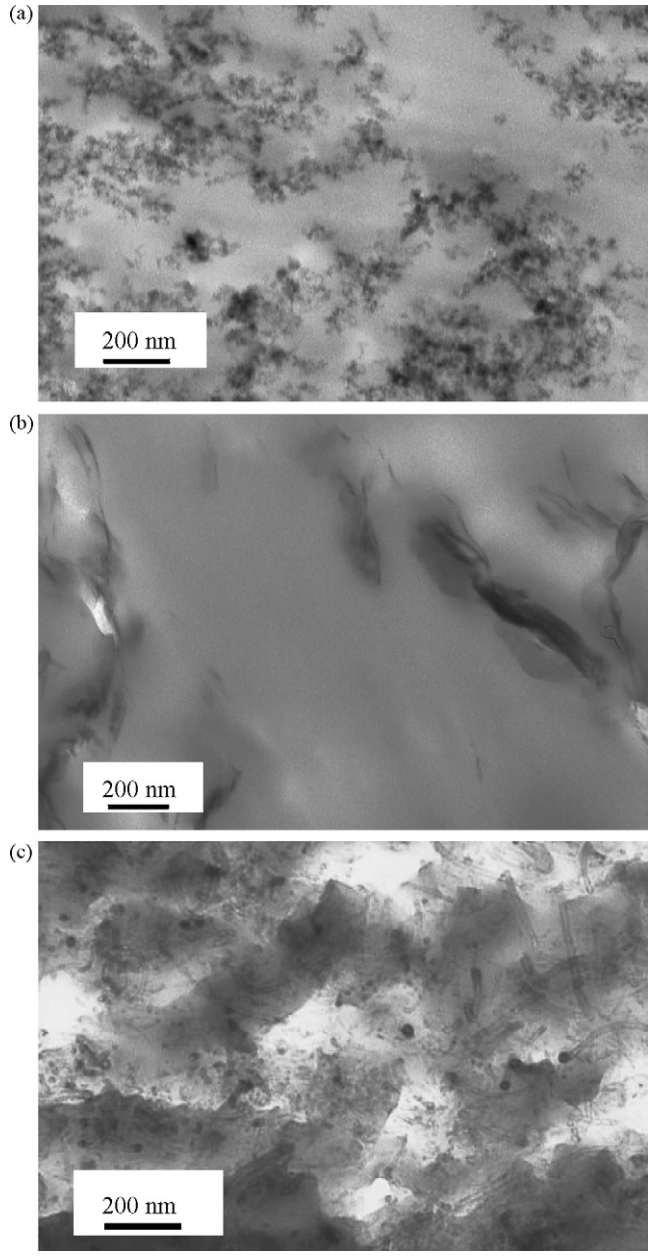

Fig. 1. TEM micrographs of PLA nanocomposites (a) PLA/SiO_2, (b) PLA/MMT and (c) PLA/MWCNT.

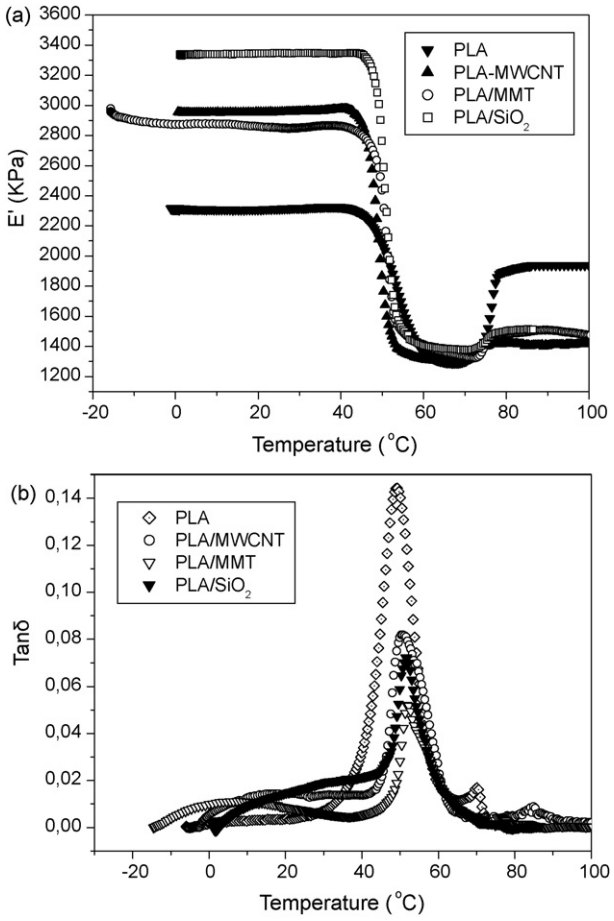

Fig. 2. Dynamic mechanical relaxation behaviour of the prepared PLA nanocomposites: (a) storage modulus (E') and (b) tan δ.

The storage modulus of neat PLA remains stable till 45 °C and decreases at temperatures close to glass transition. However, after this temperature area, storage modulus increases slightly again, with increasing temperature. This is unusual in polymers since storage modulus decreases gradually with increasing temperature. However, the recorded increase in the studied materials can be attributed to the cold-crystallization of PLA. A similar behavior can be seen also in all nanocomposites. The most characteristic difference is that the storage modulus of PLA nanocomposites is larger than neat PLA. This indicates the effectiveness of the nanopartciles on reinforcing PLA. PLA nanocomposites containing SiO_2 have the largest storage modulus, maybe because, as was also supposed by others, hydrogen bonding interaction between C=O of PLA with Si–OH of SiO_2 can take place, increasing the adhesion of nanoparticles with polymer matrix [28].

A lot of alterations were also recorded in tan δ curves. Neat PLA was found to have a T_g at 49 °C (Fig. 2b), while the temperature of the maximum remains stable or shifts to slightly higher values in case of nanocomposites. Usually the T_g of a polymeric matrix tends to increase with the addition of nanoparticles, due to the interactions between the polymer chains and the nanoparticles and to the reduction of macromolecular chain mobility at the zone surrounding the nanoparticles [29,30]. This is clearer comparing the peak areas of neat PLA and nanocomposites, which is drastically decreased after the addition of nanoparticles. The glass transition is a complex phenomenon depending on a number of factors such as chain flexibility, molecular weight, branching, cross-linking, intermolecular interactions, and steric effects. The small increase of T_g (1–2 °C) after the addition of SiO_2 could be attributed to the decrease in free volume in the polymer matrix due to the physical cross-linking caused by the interactions taking place between the silanoil groups of SiO_2 and PLA. A similar increase was reported also in PLA/MWCNTs nanocomposites due to the existence of rigid MWCNTs incorporated into the PLA matrix [31] or by using other nanoparticles like clay [32]. However, in our study it seemed that the chain segment mobility of the PLA phase was not influenced drastically by the introduction of SiO_2 or MMT nanoparticles.

Finally, as will be discussed below, the T_g values of nanocomposites measured from DSC scans of quenched nanocomposite samples were also found to increase by 1–2 °C compared to neat PLA.

3.2. Non-isothermal melt crystallization

In order to investigate the effect of the filler nanoparticles on the crystallization of the PLA matrix, crystallization tests on cooling

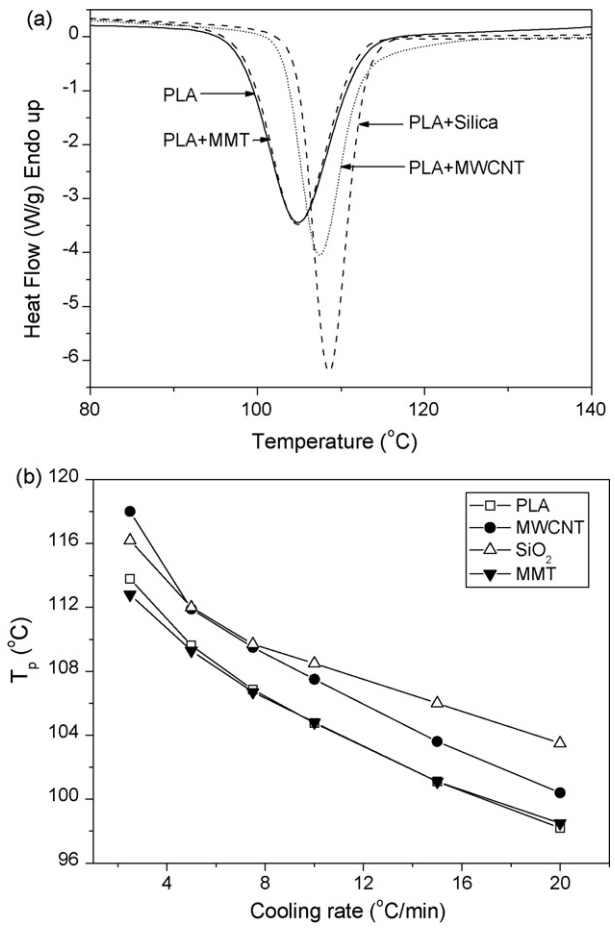

Fig. 3. (a) Typical DSC scans for melt crystallization of plain PLA and all the nanocomposites at 10 °C/min cooling rate and (b) crystallization peak temperature as a function of the cooling rate for PLA and all the nanocomposites.

from the melt or heating from the glassy state at various rates were performed using DSC.

3.2.1. Non-isothermal melt crystallization kinetics

First, non-isothermal melt crystallization was studied on cooling at various rates from 2.5 to 20 °C/min. From non-isothermal crystallization experiments, data for the crystallization exotherms as a function of temperature can be obtained, at each cooling rate. The crystallization peak becomes broader and it shifts to lower temperatures with increasing cooling rate. Typical comparative plots for plain PLA and the nanocomposites at 10 °C/min cooling rate appear in Fig. 3a. From a first look it appears that crystallization of PLA is similar to that of PLA/MMT nanocomposites, while both start and complete always at lower temperatures compared to the other nanocomposites of PLA with silica and MWCNT. Also, form a first look it appears that in the PLA/MWCNT nanocomposites a different crystallization mechanism is observed at early degrees of crystallization.

The peak temperature, T_p as a function of the cooling rate for all samples investigated appear in Fig. 3b. As it is expected, with increasing cooling rate the peak temperature decreased, meaning that the higher the cooling rate the lower the temperature that the crystallization process started and completed. Also, as it can be seen in Fig. 3b the T_p of plain PLA is similar to that of PLA/MMT nanocomposites at all cooling rates, while the T_p of the PLA/SiO_2 nanocomposites seems to be higher followed by the PLA/MWCNT nanocomposite.

Table 1
Characteristic rate constant, k and exponent, n of the Avrami equation for plain PLA and the nanocomposites.

Cooling rate (°C/min)	Plain PLA		PLA/SiO_2		PLA/MMT	
	K_A (min^{-1})	n	K_A (min^{-1})	n	K_A (min^{-1})	n
2.5	0.2165	4.17	0.2719	5.30	0.3022	4.14
5	0.3840	4.77	0.4273	6.15	0.4966	4.52
7.5	0.5015	4.69	0.5906	6.48	0.6325	4.33
10	0.6191	4.45	0.8410	5.76	0.7590	3.93
15	0.7485	3.84	1.0963	5.32	0.9193	3.08
20	0.8778	3.42	1.3909	4.33	1.0288	2.93

From the data for the crystallization exotherms as a function of temperature dH_c/dT the relative crystallinity as a function of temperature $X(T)$ can be calculated as follows:

$$X(T) = \frac{\int_{T_o}^{T_c}(dH_c/dT)dT}{\int_{T_o}^{T_\infty}(dH_c/dT)dT} \quad (1)$$

where T_o denotes the initial crystallization temperature and T_c, T_∞ the crystallization temperature at time t and after the completion of the crystallization process, respectively.

The crystallization temperature T_c, can be converted to crystallization time, t, with the well-known relationship for non-isothermal crystallization processes: [33]

$$t = \frac{(T_c - T_o)}{\beta} \quad (2)$$

where β is the constant cooling rate.

To quantitatively describe the evolution of the crystallinity during non-isothermal crystallization, a number of models have been proposed in the literature [34]. The most common approach is that based on the modified Avrami equations. According to this method, the relative degree of crystallinity, X, can be calculated from:

$$X = 1 - \exp(-Z_t t^n) \text{ or } \quad X = 1 - \exp[-(K_A t)^n] \quad (3)$$

where Z_t and n denote the growth rate constant and the Avrami exponent, respectively. Since the units of Z_t are a function of n, Eq. (3) can be written in the composite – Avrami form using K_A instead of Z_t (where $Z_t = K_A{}^n$) [35].

K_A and n can be calculated by fitting the experimental data to the following equation obtained after taking the logarithm of both sides of Eq. (3).

$$\log[-\ln(1-X)] = n\ \log(K_A) + n\log(t) \quad (4)$$

In Fig. 4 typical plots of $\log\{-\ln(1-X)\}$ versus $\log(t)$ are shown for the PLA/MMT (a) and PLA/MWCNT (b) samples. Straight lines were obtained in each cooling rate for the PLA and PLA/MMT and PLA/SiO_2 nanocomposites, while a break in the curves was clear in the PLA/MWCNT nanocomposites. From the slope and intercept of each line n and $\log(K_A)$ can be calculated and the best fitting values for the parameters n and K_A are presented in Table 1. The values of K_A as it was expected increased with the cooling rate, while n was in the vicinity of 4.2, 5.5 and 3.8 for PLA, PLA/SiO_2 and PLA/MMT, respectively. Since, for the PLA/MWCNT nanocomposite a significant deviation from linearity appeared at different values of relative degree of crystallinity, two consecutive Avrami plots were used. This way, two sets of parameters were found, associated with the primary and secondary crystallization respectively, which are reported in Table 2 together with the relative degree of crystallinity where the break points appear. The increase of n values in cases of PLA/SiO_2 and PLA/MWCNT nanocomposites indicates changes in crystallization mechanism due to heterogeneous nucleation of PLA caused by the nanoparticles.

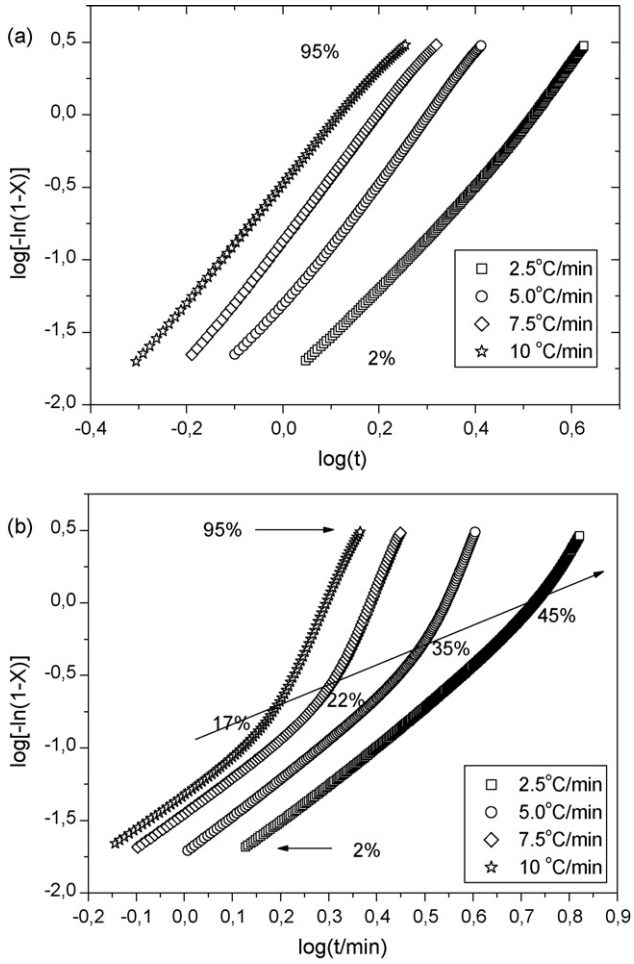

Fig. 4. Avrami-type plots for the (a) PLA/MMT and (b) PLA/MWCNT nanocomposites.

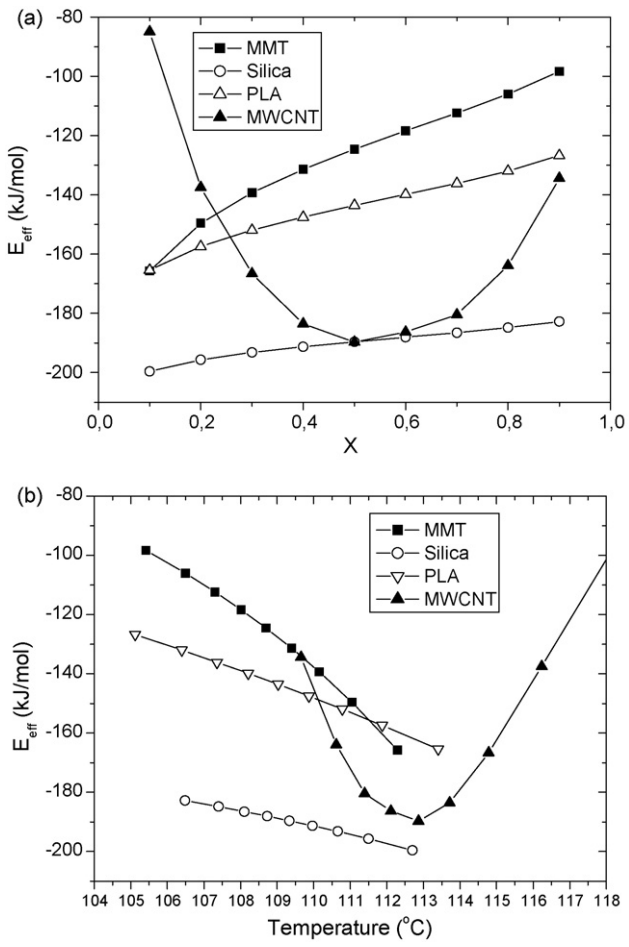

Fig. 5. Effective activation energy as a function of the relative degree of crystallinity (a) or temperature (b) obtained during melt crystallization of plain PLA and the PLA/SiO_2, PLA/MMT and PLA/MWCNT nanocomposites.

3.2.2. *Effective activation energy*

Effective activation energy is an important parameter associated with non-isothermal crystallization, as it determines the rate of the process. The effective activation energy of non-isothermal crystallization was estimated for all samples investigated. Several mathematical procedures have been proposed in literature for the calculation of the effective activation energy of non-isothermal crystallization (ΔE), considering the variation of the peak temperature with the cooling rate, β, such as the Kissinger's method which has been widely applied in evaluating the overall effective activation energy [36]. However, use of multiple heating rate methods such as isoconversional methods is recommended. An isoconversional method can in principle be applied to non-isothermal crystallizations for evaluating the dependence of the effective activation energy on conversion and temperature. The differential isoconversional method of Friedman [37] and the advanced integral isoconversional method of Vyazovkin [38–40] are the most appropriate. In this investigation the method of Friedman was used. According to the differential isoconversional method of Friedman, different effective activation energies are calculated for every degree of crystallinity from [37]:

$$\ln\left(\frac{dX}{dt}\right)_{X,i} = \text{Const} - \frac{\Delta E_X}{RT_{X,i}} \quad (5)$$

where dX/dt is the instantaneous crystallization rate as a function of time at a given conversion X, ΔE_X is the effective activation energy at a given conversion X, $T_{X,i}$ is the set of temperatures related to a given conversion X at different cooling rates, β_i and the subscript i refers to every individual cooling rate used.

According to this method, the $X(t)$ function obtained from the integration of the experimentally measured crystallization rates is initially differentiated with respect to time to obtain the instantaneous crystallization rate, dX/dt. Furthermore, by selecting appropriate degrees of crystallinity (i.e. from 5% to 95%) the values of dX/dt at a specific X are correlated to the corresponding crystallization temperature at this X, i.e. T_X. Then by plotting the left hand side of Eq. (5) with respect to $1/T_X$ a straight line must be obtained with a slope equal to $\Delta E_X/R$. In every X for cooling rates ranging between 2.5 and 10 °C/min almost linear curves were obtained. The effective activation energy, thus obtained was subsequently plotted as a function of the relative degree of crystallinity, as one can see in Fig. 5a. The effective activation energy increases with X as it has also been observed in other systems. Moreover, it was observed that the nanocomposites of PLA/SiO_2 presents always lower ΔE values compared to plain PLA and PLA/MMT, meaning a faster crystallization

Table 2
Characteristic rate constants, $K_{A,1}$ and $K_{A,2}$ and exponents, n_1 and n_2 of the Avrami equation for the PLA/MWCNT nanocomposite.

Cooling rate (°C/min)	PLA/MWCNT				
	$K_{A,1}$ (min^{-1})	n_1	$K_{A,2}$ (min^{-1})	n_2	X at break
2.5	0.1642	2.56	0.1852	5.04	45
5	0.2201	2.63	0.2865	7.69	35
7.5	0.2608	2.47	0.4107	7.80	22
10	0.2831	2.39	0.5063	7.45	17

rate as it was observed from the DSC measurements. The effective activation energy of PLA/MWCNT is initially high decreases with increasing X, and after 50% it increases again. Finally, by taking an average temperature at each X, the effective activation energy can be plotted as a function of temperature shown in Fig. 5b. ΔE decreases with temperature for PLA, PLA/SiO_2 and PLA/MMT, while it initially decreases but then increases for PLA/MWCNT.

3.2.3. Nucleation activity

Dobreva and Gutzow [41,42] suggested a simple method for calculating the nucleation activity of foreign substrates in polymer melt. This method has been also used for silica nanoparticle-filled PEN [43] and for PP composites [44]. Nucleation activity (φ) is a factor by which the work of three-dimensional nucleation decreases with the addition of a foreign substrate. If the foreign substrate is extremely active, φ approaches 0, while for inert particles, φ approaches 1. The nucleation activity is calculated from the ratio:

$$\varphi = \frac{B^*}{B} \tag{6}$$

where B is a parameter that can be calculated from the following equation

$$B = \frac{\omega\sigma^3 V_m^2}{3nk_B T_m^0\ \Delta S_m^2} \tag{7}$$

where ω is a geometric factor, σ is a specific energy, V_m is the molar volume of the crystallizing substance, n is the Avrami exponent, ΔS_m is the entropy of melting and T_m^0 is the infinite crystal melting temperature (assumed to be equal to 207 °C for PLA [45]).

Furthermore, B can be experimentally determined from the slope of Eq. (8) obtained by plotting $\ln(\beta)$ versus the inverse squared degree of supercooling $1/\Delta T_p^2 (\Delta T_p = T_m - T_p)$ [32,42]:

$$\ln\beta = \text{Const} - \frac{B}{\Delta T_p^2} \tag{8}$$

The above equation holds for homogeneous nucleation from a melt, near the melting temperature. By using a nucleating agent, Eq. (8) is transformed to the following for heterogeneous nucleation:

$$\ln\ \beta = \text{Const} - \frac{B^*}{\Delta T_p^2} \tag{9}$$

Plots of $\ln(\beta)$ versus $1/\Delta T_p^2$ for the plain PLA and all PLA nanocomposites are shown in Fig. 6a. As it can be seen straight lines are obtained in every sample (correlation coefficient $R > 0.998$). From the slopes of these lines, the values of B and B^* for the plain PLA and the nanocomposites can be calculated, respectively. Then, the nucleation activity is computed from Eq. (6) and is presented in Fig. 6b. From these results, it can be seen that the nanocomposite of PLA with MMT exhibited no nucleation effect, while this was clear for the other two nanocomposites, indicating that Silica and MWCNT were acting effectively as nucleation agents in the PLA matrix.

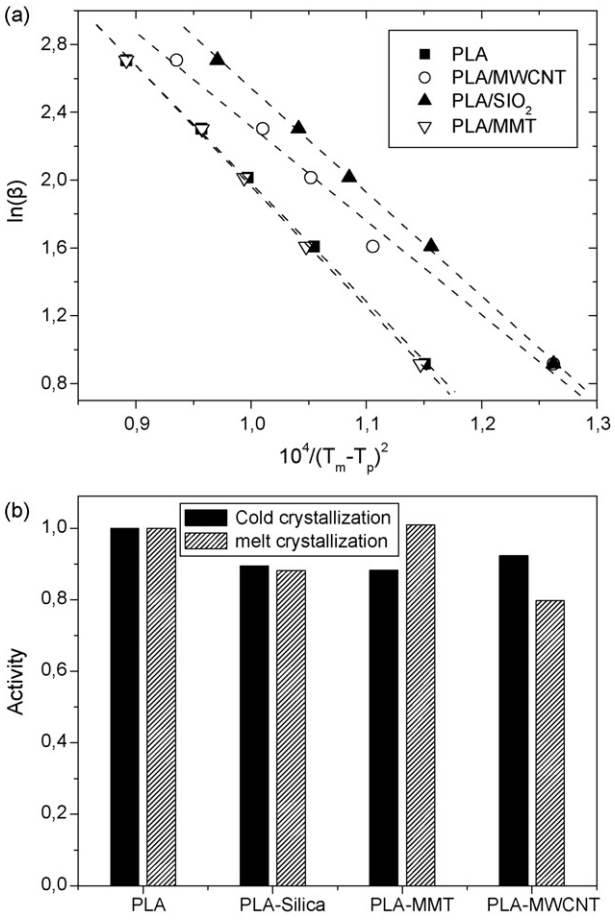

Fig. 6. (a) Plots of $\ln(\beta)$ versus $1/\Delta T_p^2$ for the plain PLA and all PLA nanocomposites and (b) nucleation activity for PLA and all PLA nanocomposites.

3.3. Non-isothermal cold-crystallization

3.3.1. Cold-crystallization kinetics

Moreover, crystallization experiments on heating were carried out for the PLA and PLA nanocomposites at different heating rates. Typical DSC scans appear in Fig. 7a. As it can be seen again for PLA nanocomposites with silica or MWCNT crystallization started at lower temperatures compared to those of plain PLA and PLA/MMT nanocomposites. However, the final crystallinity was higher for neat PLA and PLA/MMT nanocomposites as can be proved by the larger areas of melting peaks. Furthermore, for nanocomposites increased tendency for recrystallization can be observed and finally the melting peak temperature is higher as a result of crystal perfection on heating. This behavior can be attributed to nucleation due to the presence of nanofiller. Thus, crystallization initialized at lower temperatures and this resulted in generation of some imperfect crystals which then act as cross-linkings between macromolecular chains, reducing mobility and ability of chains to further crystallize, finally limiting ultimate achievable crystallinity.

The peak temperature, T_p as a function of the heating rate for all samples investigated appear in Fig. 7b. As it is expected, with increasing heating rate the peak temperature increased, meaning that the higher the heating rate the higher the temperature that the crystallization process started and completed. Also, as it can be seen in Fig. 7b that the T_p of plain PLA is higher compared to the nanocomposites followed by the PLA/MMT, PLA/MWCNT, while the T_p of the PLA/SiO_2 nanocomposites was always the lower, meaning that silica nanoparticles nucleated PLA cold-crystallization more effectively.

Following, from the data for the crystallization exotherms as a function of temperature dH_c/dT the relative crystallinity as a function of temperature $X(T)$ can be calculated from an equation similar to Eq. (1), and the crystallization temperature T_c, can be converted to crystallization time, t, from Eq. (2). Then, by taking the inverse of the half crystallization time (meaning the time to achieve 50% relative degree of crystallinity) a measurement of the crystallization rate can be obtained. Such plots appear in Fig. 8a.

From Fig. 8a, it can be observed that the nanocomposites of PLA with MWCNT exhibit the lower crystallization rate. In order to quantitatively describe the evolution of the crystallinity during non-isothermal crystallization the modified Avrami equation (3)

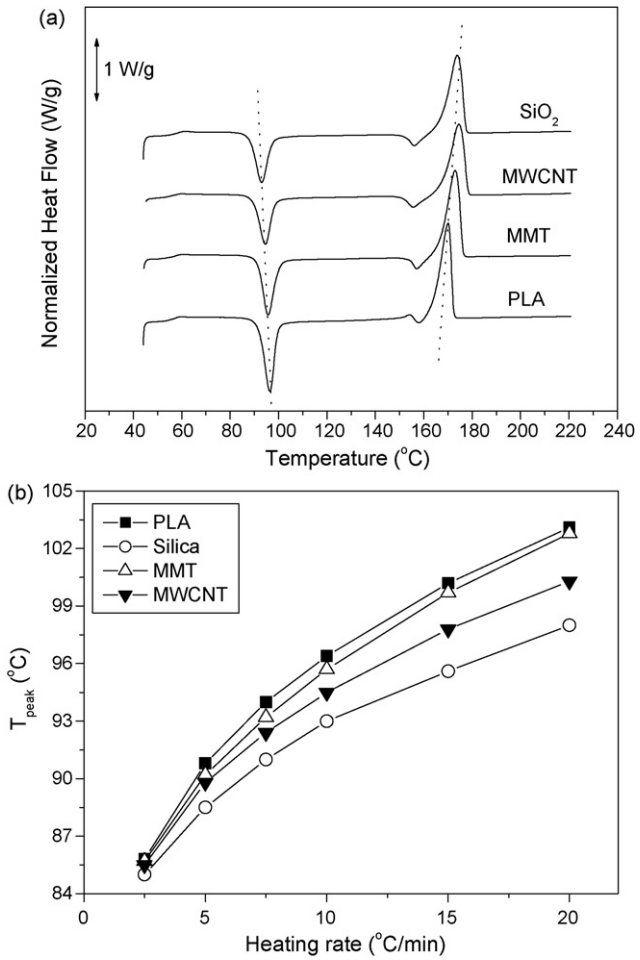

Fig. 7. (a) Typical DSC scans for cold-crystallization of plain PLA and all the nanocomposites at 10 °C/min heating rate and (b) crystallization peak temperature as a function of the heating rate for PLA and all the nanocomposites.

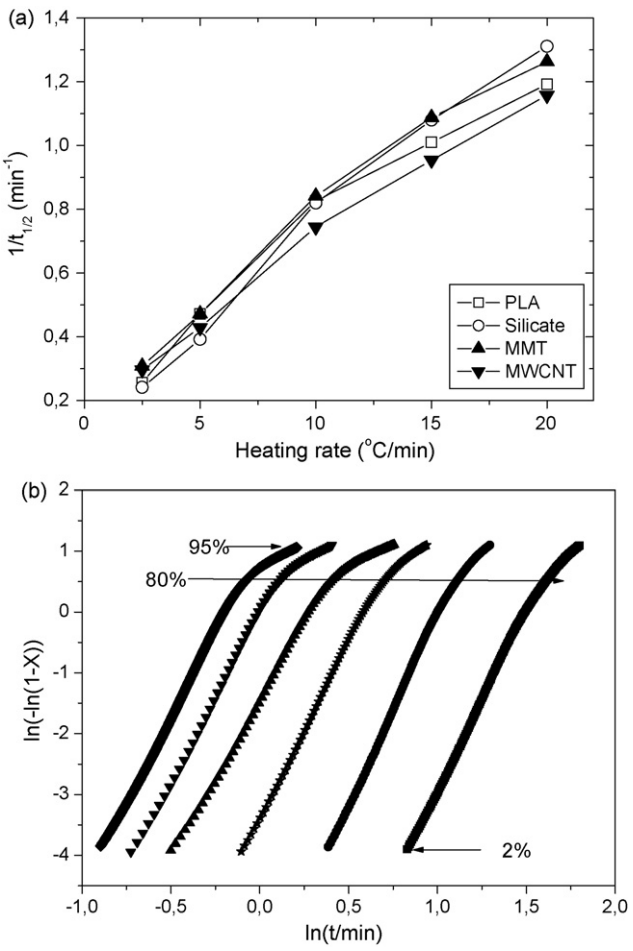

Fig. 8. (a) Inverse of the half crystallization time as a function of the heating rate for PLA and all the nanocomposites and (b) Avrami-type plots for the cold-crystallization of PLA/SiO_2 nanocomposites at different heating rates.

was used. In Fig. 8b typical plots of $\log\{-\ln(1-X)\}$ versus $\log(t)$ are shown for the PLA/SiO_2 samples. Straight lines were obtained in each cooling rate until approximately 80% relative degree of crystallinity meaning a secondary nucleation mechanism after that point. From the slope and intercept of each line n and $\log(K_A)$ can be calculated and the best fitting values for the parameters n and K_A are presented in Table 3. The values of K_A as it was expected increased with the cooling rate, while n was in the vicinity of 5.9, 5.8, 5.6 and 5.9 for PLA, PLA/SiO_2, PLA/MWCNT and PLA/MMT, respectively.

3.3.2. *Effective activation energy of cold-crystallization*

The effective activation energy of non-isothermal cold-crystallization was estimated for all samples investigated, according to the Friedman's method and the procedure described in the melt crystallization section. The effective activation energy, thus obtained, was subsequently plotted as a function of the relative degree of crystallinity, as one can see in Fig. 9a. The effective activation energy either increases or decreases with X depending on the particular specimen. Moreover, it was observed that the PLA/SiO_2 nanocomposites present always higher ΔE values compared to other samples. Finally, by taking an average temperature at each X, the effective activation energy can be plotted as a function of temperature shown in Fig. 9b. The same tendency is observed, but it is clear in these plots that crystallization occurred at lower temperatures for PLA/SiO_2 and PLA/MWCNT and the imperfect crystals generated at low temperatures as discussed above reduced chain mobility and thus crystallizability of the PLA matrix. It must be also noted here that the T_g in case of PLA/SiO_2 nanocomposites increased, showing a reduction in chain mobility, which in turn is expected to cause an increase in effective activation energy of cold-crystallization. In contrast, MMT nanoparticles had a smaller

Table 3
Characteristic rate constant, k and exponent, n of the Avrami equation for plain PLA and the nanocomposites.

Heating rate (°C/min)	Plain PLA		PLA/SiO_2		PLA/MWCNT		PLA/MMT	
	K_A (min^{-1})	n	K_A (min^{-1})	n	K_A (min^{-1})	n	K_A (min^{-1})	n
2.5	0.4355	4.2	0.2241	5.9	0.2753	5.2	0.2983	5.5
5	0.5041	5.9	0.3661	6.3	0.4046	6.2	0.4561	6.9
7.5	0.6247	6.3	0.5559	5.8	0.7596	4.2	0.6506	5.1
10	0.7761	6.1	0.7559	5.2	0.8477	4.7	0.8943	5.2
15	0.9544	6.5	1.0011	5.6	0.8939	6.6	1.0230	6.2
20	1.1246	6.5	1.2174	5.7	0.9232	6.7	1.2502	6.3

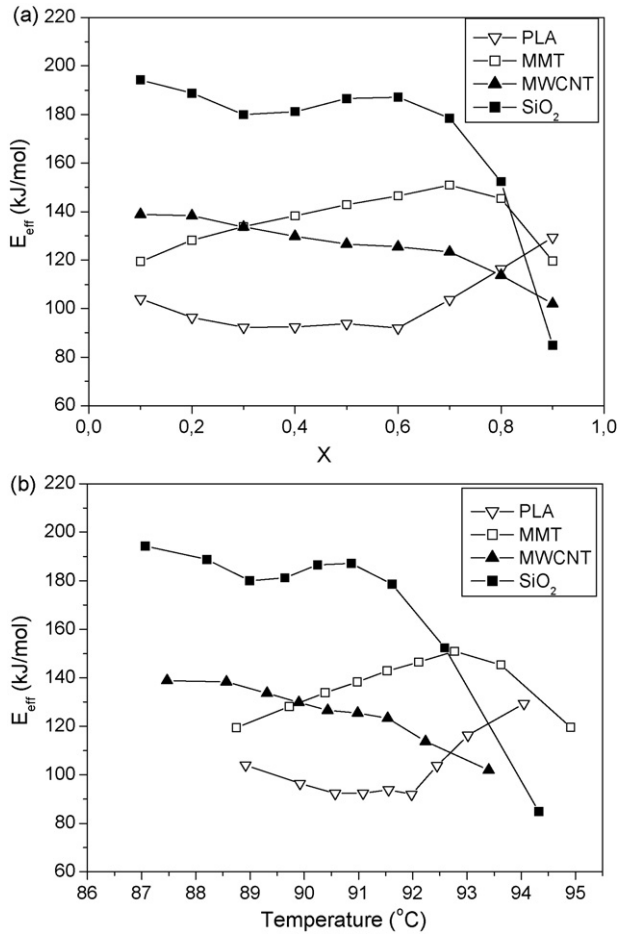

Fig. 9. Effective activation energy as a function of the relative degree of crystallinity (a) or temperature (b) obtained during cold-crystallization of plain PLA and the PLASiO_2, PLA/MMT and PLA/MWCNT nanocomposites.

size as was reported in the experimental. This might be responsible for a less significant influence of their addition in PLA matrix on the crystallization, meaning both effective activation energy and nucleation activity of the MMT nanoparticles.

3.3.3. Nucleation activity

Moreover, the nucleation activity of foreign substrates in polymer melt was estimated for cold-crystallization using the method of Dobreva and Gutzow [42], properly modified. Then, φ was estimated from Eqs. (6), (8) and (9), but in place of ΔT the following assumption was made: since it is a cold-crystallization the temperature difference of the crystallization temperature from the glass transition temperature is the determining parameter and not the difference from the equilibrium melting point of the polymer. Thus, instead of using the equilibrium melting point the glass transition temperature for each sample at every cooling rate was used, i.e. $\Delta T_p = T_p - T_g$. Values of T_g for all samples and heating rates appear in Table 4.

Accordingly, parameters B and B^* were obtained from the plots of $\ln(\beta)$ versus $1/\Delta T_p^2$ for the plain PLA and all PLA nanocomposites as it can be shown in Fig. 10. Again, very good straight lines were obtained in every sample (correlation coefficient $R > 0.998$). From the slopes of these lines, the values of B and B^* for the plain PLA and the nanocomposites can be calculated, respectively. Then, the nucleation activity was computed from Eq. (6) and it is included in Fig. 10, in comparison to those values obtained from melt crystallization experiments. From these results, it can be seen that the

Table 4
Glass transition temperature (°C) of PLA and all nanocomposites.

Heating rate (°C/min)	PLA	PLA/SiO_2	PLA/MMT	PLA/MWCNT
2.5	54.4	55.1	54.9	55.2
5.0	55.1	56.9	55.9	55.8
7.5	56.2	57.8	56.9	56.4
10	56.7	58.1	57.5	56.6
15	57.1	58.6	57.8	56.8
20	57.7	59.0	58.4	57.1

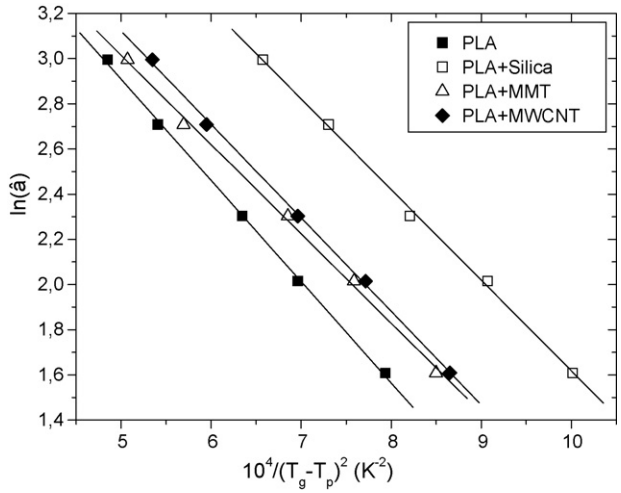

Fig. 10. Plots of $\ln(\beta)$ versus $1/\Delta T_p^2$ for the plain PLA and all PLA nanocomposites.

MMT and silica nanoparticles exhibited the best nucleation effect on PLA matrix.

3.4. Lauritzen–Hoffman analysis

In the literature it has been proposed that the spherulite growth rate as a function of temperature and cooling rate in non-isothermal crystallization can be described by a modified Lauritzen–Hoffman equation [33,46]. In this study analyze DSC non-isothermal melt crystallization data were also by this modified model.

According to the secondary nucleation theory of Lauritzen and Hoffman the spherulitic growth rates can be expressed as: [47]

$$G = G_o \exp\left[\frac{-U^*}{R(T_c - T_\infty)}\right] \exp\left[\frac{-K_g}{T_c(\Delta T)f}\right] \quad (10)$$

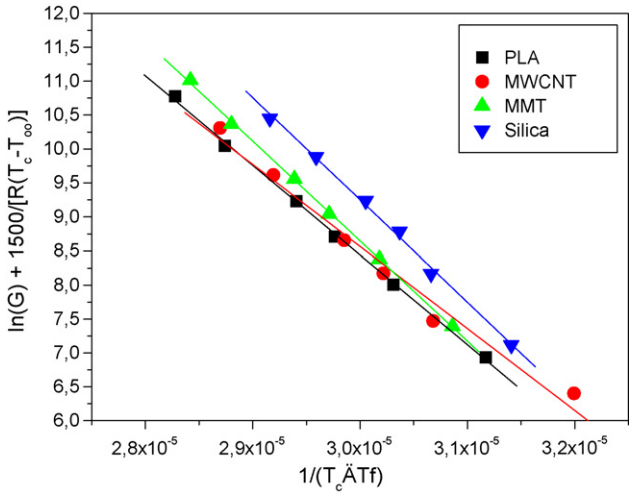

Fig. 11. Lauritzen–Hoffmann plots for neat PLA and the PLA nanocomposites.

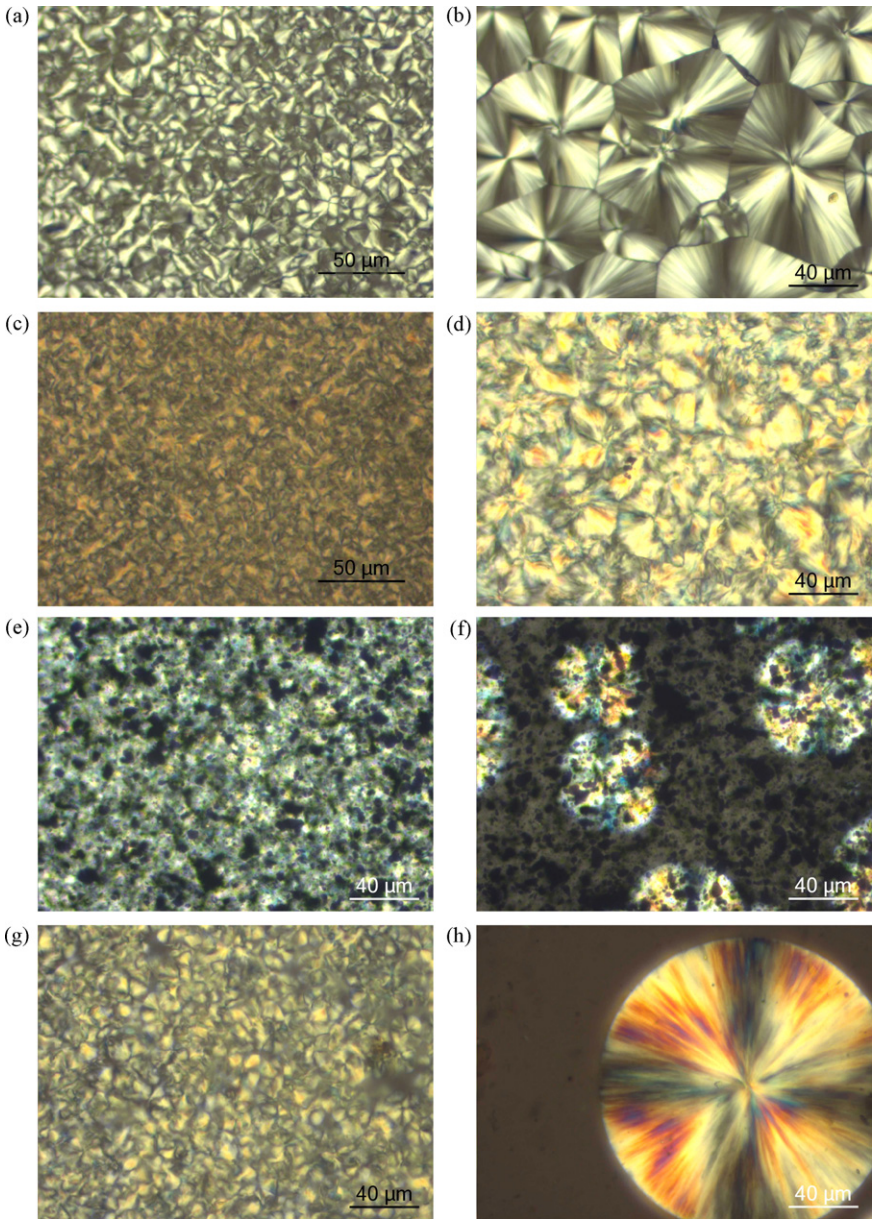

Fig. 12. PLM photographs showing the morphology generated on crystallization from the melt for neat PLA and PLA nanocomposites: (a) PLA 100 °C, (b) PLA 120 °C, (c) PLA/MMT 100 °C, (d) PLA/MMT 120 °C, (e) PLA/MWCNT 120 °C, (f) PLA/MWCNT 135 °C, (g) PLA/SiO_2 120 °C, and (h) PLA/SiO_2 130 °C.

where, G_0 is the pre-exponential factor, the first exponential term contains the contribution of diffusion process to the growth rate, while the second exponential term is the contribution of the nucleation process; U^* denotes the activation energy which characterizes molecular diffusion across the interfacial boundary between melt and crystals, usually set equal to 1500 cal/mol and this was the case in this work and T_∞ is the temperature below which diffusion stops, usually equal to $T_\infty = T_g - 30$ K; K_g is a nucleation constant and ΔT denotes the degree of undercooling ($\Delta T = T_m^0 - T_c$); f is a correction factor which is close to unity at high temperatures and is given as $f = 2T_c/(T_m^0 + T_c)$; the equilibrium melting temperature, T_m^0 was set equal to 207 °C for PLA, while the glass transition temperature slightly varied for nanocomposites as will be discussed in the next section [45]. Eq. (10) can be also written as follows:

$$\log G + \frac{U^*}{2.303R(T_c - T_\infty)} = \log G_o - \frac{K_g}{2.303T_c(\Delta T)f} \quad (11)$$

Plotting the left-hand side of Eq. (11) with respect to $1/(T_c(\Delta T)f)$ a straight line should appear having a slope equal to K_g. Fig. 11 gives the plots for the PLA nanocomposites and neat PLA. These plots can give K_g as a slope and the intercept of $\ln G_0$.

Here, growth rate G, which should be obtained essentially by the spherulite growth, was calculated by the inverse of crystallization half time ($t_{1/2}$) [33]. Thus, the following data are mainly for the purpose of qualitative comparison between PLA matrix and its nanocomposites. Actually, this substitution has been widely used in crystallization study of both the polymers and their composite systems.

The resulting K_g values were 1.32×10^6 for neat PLA, and varied to 1.2×10^6 for PLA/MWCNT, to 1.47×10^6 for PLA/MMT and finally to 1.5×10^6 for PLA/SiO_2 nanocomposites.

Generally, the crystallization of polymers proceeds in three regimes. In regime I, the crystal growth rate G varies with the surface nucleation rate I ($G \propto i$). With an increase in the nucleation rate (regime II), multiple nucleation occurs on the substrate ($G \propto i^{1/2}$).

In a high-rate nucleating stage (regime III), the mean separation of nuclei on the substrate approaches the width of molecular stems (again, $G \propto i$). The Lauritzen Z test is usually employed to investigate to which regime the K_g data in the selected temperature region belonged. Z is defined as:

$$Z \cong 10^3 \left(\frac{L}{2\alpha_0}\right) \exp\left[\frac{-X}{T_c \Delta T}\right] \quad (12)$$

where L is the effective lamellar thickness and a_0 is the chain stem width. Regime I kinetics are followed if substitution of $X = K_g$ into Eq. (10) results in $Z \leq 0.01$. If $X = 2K_g$, Eq. (15) yields $Z \geq 1$, and then regime II are followed. Besides, many researchers have in detail investigated the temperature region in which regime transition occurs and it was concluded that, at the T_c ranges below and above 120 °C, the PLA crystallizes according to regime III and regime II kinetics, respectively.

Thus, according to the DSC data showed in Fig. 11, for the neat PLA and its nanocomposites, the non-isothermal crystallization from the melt proceeds by regime III kinetics.

For a secondary or heterogeneous nucleation, K_g can be calculated from:

$$K_g = \frac{n\sigma\sigma_e b_0 T_m^0}{\Delta h_f \rho_c k_B} \quad (13)$$

where, n is a constant equal to 4 for regime I and III and 2 for regime II, σ, σ_e are the side surface (lateral) and fold surface (end) free energies which measure the work required to create a new surface, b_0 is the single layer thickness, $\Delta h_f \times \rho_c = \Delta H_f$ is the enthalpy of melting per unit volume and it was assumed to be 1.1×10^8 J/m^3 for PLA and k_B is the Boltzmann constant ($k_B = 1.38 \times 10^{-23}$ J/K).

The resulting value for the product $\sigma\sigma_e$ using K_{gIII} was $\sigma\sigma_e = 20.4 \times 10^{-4}$ J^2/m^4 for neat PLA, $\sigma\sigma_e = 18.5 \times 10^{-4}$ J^2/m^4 in case of PLA/MWCNT, $\sigma\sigma_e = 22.7 \times 10^{-4}$ J^2/m^4 in case of PLA/MMT and $\sigma\sigma_e = 23.1 \times 10^{-4}$ J^2/m^2 in case of PLA/SiO_2 nanocomposite.

3.5. PLM observations during melt crystallization

PLM was used to directly study morphology of the nanocomposites during melt crystallization. Thus thin films were observed during isothermal crystallization from the melt. As can be seen in photos of Fig. 12, the nanocomposites showed increased spherulite sizes compared to neat PLA. Also crystallization was faster at every temperature. This is due to the heterogeneous nucleation of nanofillers on polymer matrix [48]. Finally, peculiar morphologies were observed for the PLA/MWCNT nanocomposite.

3.6. Prediction of the dynamic fragility from glass transition

In this section the dynamic fragility of plain PLA and all nanocomposites was estimated using thermal methods according to the procedure reviewed by Crowley and Zografi [49]. Then, at a single temperature, the fragility parameter, m could be defined by:

$$m \equiv \left.\frac{d\ \log\tau}{d(T_g/T)}\right|_{T=T_g} = \frac{\Delta E_{T_g}}{(\ln\ 10)RT_g} \quad (14)$$

where τ is a mean relaxation time given by the following form of the Vogel–Tammann–Fulcher (VTF) equation [49]:

$$\tau = \tau_0\ \exp\left(\frac{DT_0}{T - T_0}\right) \quad (15)$$

τ_0, D and T_0 are constants, with D termed the strength parameter, with a large value (>30) representing 'strong' behaviour and low D value (<10) representing 'fragile' behaviour. Parameter D can be calculated by the following Eq. (12) using $m_{min} = 16$ [49]:

$$D = \frac{(\ln\ 10)m_{min}^2}{m - m_{min}} \quad (16)$$

In Eq. (10), ΔET_g was assumed equal to the average effective activation energy ΔE_{ave} calculated from the variation of T_g with the heating rate. In order to determine an average effective activation energy ΔE_{ave} Moynihan et al. [50] have proposed the use of a dependence of the T_g on the rate of heating or cooling as

$$\frac{\Delta E_{ave}}{R} = -\frac{d(\ln\ |\beta|)}{d(1/T_g)} \quad (17)$$

For heating, Eq. (17) is applicable subject to the constraint that prior to heating the glassy material should be cooled from above to well below the glass transition region at a rate whose absolute value is equal to the rate of heating.

From the values of T_gs presented in Table 4 and Eq. (17) the average effective activation energy was estimated for all samples from the plots of Fig. 13. The resulted values appear in Table 5. The fragility, m estimated from Eq. (10) appears also in the same table. A large m-value indicates rapidly changing dynamics at T_g which equates to 'fragile' behavior. As it can be seen the PLA + MWCNT nanocomposites seem to be much more fragile compared to all other specimens. Furthermore, parameter D was calculated form Eq. (16) and the values are included in Table 5. All values of D are lower than 10 meaning a fragile behavior, which however is typical for polymeric materials.

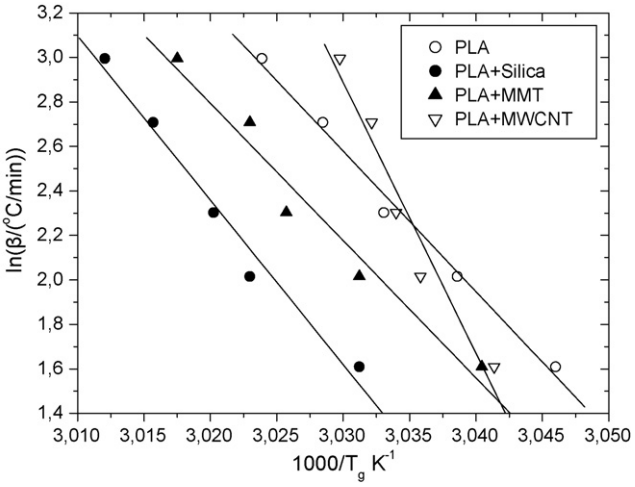

Fig. 13. Plot of ln(β) as a function of $1/T_g$.

Table 5
Fragility parameters.

Sample	DE_{T_g} (Kj/mol)	T_g (°C)	m	D
PLA	525.4	56.6	83.27	8.76
PLA/SiO_2	614.4	58.1	96.94	7.28
PLA/MMT	513.0	57.3	81.13	9.05
PLA/MWCNT	1012.6	56.5	160.52	4.08

4. Conclusions

Three different types of PLA nanocomposites were prepared. Fine dispersion of the nanoparticles was observed from SEM micrographs, while a slight increase in T_g values was also evidenced from tan δ vs temperature plots after DMA measurements. Furthermore, the nanoparticles showed some nucleation activity referring to non-isothermal crystallization from the melt or from the glassy state. On cooling from the melt crystallization was found to start

at higher temperature in nanocomposites, especially in the presence of silica nanoparticles or MWCNT. Effective activation energy was found lower in such cases, after calculations following the isoconversional method of Friedmann. The method proposed by Dobreva was applied and it proved some nucleation activity of the nanofillers. Cold-crystallization was also investigated. However, in this case crystallization occurred at lower temperatures proving the nucleation activity of the fillers, but it resulted in formation of some imperfect crystalline structure which seems to limit the ultimate crystallinity that could be achieved during the heating scan in the DSC. The findings were also proved by PLM observations since the matrix in the nanocomposites could crystallize at higher temperatures, giving larger spherulites than in neat PLA.

References

[1] J.W. Park, S.S. Im, J. Appl. Polym. Sci. 86 (2002) 647–655.
[2] C.S. Proikakis, N.J. Mamouzelos, P.A. Tarantili, A.G. Andreopoulos, Polym. Degrad. Stab. 91 (2006) 614–619.
[3] A.P. Gupta, V. Kumar, Eur. Polym. J. 43 (2007) 4053–4074.
[4] T. Maharana, B. Mohanty, Y.S. Negi, Prog. Polym. Sci. 34 (2009) 99–124.
[5] L.T. Lim, R. Auras, M. Rubino, Prog. Polym. Sci. 33 (2008) 820–852.
[6] B. Gupta, N. Revagade, J. Hilborn. Prog. Polym. Sci. 32 (2007) 455–482.
[7] M.S. Taylor, A.U. Daniels, K.P. Andriano, J. Hellert, J. Appl. Biomater. 5 (1994) 151–157.
[8] J.M. Lagaron, L. Cabedo, D. Cava, J.L. Feijoo, R. Gavara, E. Gimenez, Food Addit. Contamin. 22 (2005) 994–998.
[9] J.H. Chang, Y.U. An, D. Cho, E.P. Giannelis, Polymer 44 (2003) 3715–3720.
[10] V. Siracusa, P. Rocculi, S. Romani, M. Dalla, Rosa. Trends Food Sci. Technol. 19 (2008) 634–643.
[11] V.J. Chen, L.A. Smith, P.X. Ma, Biomaterials 27 (2006) 3973–3979.
[12] R. Kotek, Polym. Rev. 48 (2008) 221–229.
[13] H. Li, M.A. Huneault, Polymer 48 (2007) 6855–6866.
[14] L. Jiang, M.P. Wolcott, J. Zhang, Biomacromolecules 7 (2006) 199–207.
[15] S.I. Marras, I. Zuburtikudis, C. Panayiotou, Eur. Polym. J. 43 (2007) 2191–2206.
[16] M. Murariu, A. Da Silva Ferreira, P. Degee, M. Alexandre, P. Dubois, Polymer 48 (2008) 2613–2618.
[17] S.S. Ray, M. Okamoto, Prog. Polym. Sci. 28 (2003) 1539–1641.
[18] J.Y. Nam, S.S. Ray, M. Okamoto, Macromolecules 36 (2003) 7126–7131.
[19] P. Bordes, E. Pollet, L. Avirous, Prog. Polym. Sci. 34 (2009) 125–155.
[20] J. Njuguna, K. Pielichowski, S. Desai, Polym. Adv. Technol. 19 (2008) 947–959.
[21] D.R. Paul, L.M. Robeson, Polymer 49 (2008) 3187–3204.
[22] K.W. Putz, M.J. Palmeri, R.B. Cohn, R. Andrews, L.C. Brinson, Macromolecules 4 (2008) 6752–6756.
[23] A. Okada, A. Usuki, Macromol. Mater. Eng. 291 (2006) 1449–1476.
[24] H. Zou, S. Wu, J. Shen. Chem. Rev. 108 (2008) 3893–3957.
[25] D. Bikiaris, A. Vassiliou, K. Chrissafis, K.M. Paraskevopoulos, A. Jannakoudakis, A. Docoslis, Polym. Degrad. Stab. 93 (2008) 952.
[26] S. Yan, J. Yin, Y. Yang, Z. Dai, J. Ma, X. Chen, Polymer 48 (2007) 1688–1694.
[27] C.S. Wu, H.T. Liao, J. Appl. Polym. Sci. 109 (2008) 2128–2138.
[28] X. Wen, Y. Lin, C. Han, K. Zhang, X. Ran, Y. Li, L. Dong, J. Appl. Polym. Sci. 114 (2009) 3379–3388.
[29] K. Chrissafis, K.M. Paraskevopoulos, G.Z. Papageorgiou, D.N. Bikiaris, Appl. Polym. Sci. 110 (2008) 1739–1749.
[30] K. Chen, C.A. Wilkie, S. Vyazovkin, J. Phys. Chem. B 111 (2007) 12685–12692.
[31] J.T. Yoon, Y.G. Jeong, S.C. Lee, B.G. Min, Polym. Adv. Technol. 20 (2009) 631–638.
[32] P. Krishnamachari, J. Zhang, J. Lou, J. Yan, L. Uitenham, Int. J. Polym. Anal. Charact. 14 (2009) 336–350.
[33] D.S. Achilias, G.Z. Papageorgiou, G.P. Karayannidis, J. Polym. Sci.: Polym. Phys. 42 (2004) 3775–3796.
[34] M.L. Di Lorenzo, C. Silvestre, Prog. Polym. Sci. 24 (1999) 917–950.
[35] G.Z. Papageorgiou, D.S. Achilias, D.N. Bikiaris, Macromol. Chem. Phys. 208 (2007) 1250–1264.
[36] H.E. Kissinger, J. Res. Natl. Bur. Stand. 57 (1956) 217–221.
[37] H. Friedman, J. Polym. Sci. Part C 6 (1964–1965) 183–190.
[38] S. Vyazovkin, N. Sbirrazzuoli, J. Phys. Chem. B107 (2003) 882–888.
[39] S. Vyazovkin, I. Dranca, Macromol. Chem. Phys. 207 (2006) 20–25.
[40] S. Vyazovkin, N. Sbirrazzuoli, Macromol. Rapid Commun. 25 (2004) 733–738.
[41] A. Dobreva, I. Gutzow, J. Non-Cryst. Solids 162 (1993) 1–12.
[42] A. Dobreva, I. Gutzow, J. Non-Cryst. Solids 162 (1993) 13–25.
[43] S.H. Kim, S.H. Ahn, T. Hirai, Polymer 44 (2003) 5625–5634.
[44] G.Z. Papageorgiou, D.S. Achilias, D.N. Bikiaris, G.P. Karayannidis, Thermochim. Acta 427 (2005) 117–128.
[45] H. Tsuji, Y. Ikada, Polymer 36 (1995) 2709–2716.
[46] B.A. Lim, K.S. McGuire, D.R. Lloyd, Polym. Eng. Sci. 33 (1993) 537–544.
[47] J.D. Hoffman, G.T. Davis, J.I. Lauritzen, in: N.B. Hannay (Ed.), Treatise on Solid State Chemistry, vol.3, Plenum, New York, 1976.
[48] D. Bikiaris, Materials 3 (2010) 2884–2946.
[49] K.J. Crowley, G. Zografi, Thermochim. Acta 380 (2001) 79–93.
[50] C.T. Moynihan, S.K. Lee, M. Tatsumisago, T. Minami, Thermochim. Acta 280/281 (1996) 153.